The DOI for this manuscript is doi: 10.1175/BAMS-D-15-00029.1

The final published version of this manuscript will replace the preliminary version at the above DOI once it is available.

If you would like to cite this EOR in a separate work, please use the following full citation:

Zhao, K., Q. Lin, W. Lee, Y. Sun, and F. Zhang, 2015: Doppler Radar Analysis of Triple Eyewalls in Typhoon Usagi (2013). Bull. Amer. Meteor. Soc. doi:10.1175/BAMS-D-15-00029.1, in press.

Doppler Radar Analysis of Triple Eyewalls in Typhoon Usagi (2013)

Kun Zhao[1] and Qing Lin

Key Lab of Mesoscale Severe Weather/Ministry of Education of China,
and School of Atmospheric Sciences, Nanjing University, Nanjing, China

Wen-Chau Lee

Earth Observing Laboratory, National Center for Atmospheric Research[2]
Boulder, Colorado

Y. Qiang Sun and Fuqing Zhang

Center for Advanced Data Assimilation and Predictability Techniques and
Department of Meteorology, the Pennsylvania State University, University Park,
Pennsylvania

4 March 2015
Submitted to Bulletin of the American Meteorological Society

Revised May, 2015

---

[1] *Corresponding Author address*: Nanjing University, 22 Hankou Road, Nanjin 210093 China. E-mail: zhaokun@nju.edu.cn

[2] National Center for Atmospheric Research is sponsored by the National Science Foundation.

Abstract

Strong tropical cyclones often undergo eyewall replacement cycles that is accompanied with concentric eyewalls and/or rapid intensity changes while the secondary eyewall contracts radially inward and eventually replaces the inner eyewall. To the best of our knowledge, the only documented partial/incomplete tertiary eyewall has been mostly inferred from two-dimensional satellite images or one-dimensional aircraft flight-level measurements that can be regarded as indirect and tangential. This study presents the first high spatial and temporal resolution Doppler radar observations of a tertiary eyewall formation event in Typhoon Usagi (2013) over a 14-hour time period before it makes landfall. The primary (tangential) and secondary (radial) circulations of Usagi deduced from the Ground-Based Velocity Track Display (GBVTD) methodology clearly portrayed three distinct axisymmetric maxima of radar reflectivity, tangential wind, vertical velocity, and vertical vorticity. Usagi's central pressure steadily deepened during the contraction of the secondary and tertiary eyewalls until the tertiary eyewall hit the coast of southeast China that terminated the intensification of Usagi.

Background

Tropical cyclones (TCs) are the most deadly storms on Earth. Intense TCs (Category 3-5 on the Saffir-Simpson scale) are capable of producing catastrophic loss of lives and property damages to coastal residents around the world. Approximately 57% of category 4 and 72% of category 5 TCs in the western North Pacific possess a double eyewall structure where a partial or complete convective ring forms surrounding the pre-existing eyewall (Kuo et al. 2009).

This convective ring is collocated with an axisymmetric tangential wind maximum and is usually defined as the secondary (or outer) eyewall (Willoughby et al., 1982). Similarly, Hawkins et al. (2006) found 80% of West Pacific intense typhoons [maximum wind > 120 kt] had concentric eyewalls. TCs with concentric eyewalls often undergo a replacement cycle in which the primary eyewall is replaced by the secondary eyewall, coinciding with characteristic intensity changes.

Passive satellite microwave imagery during 1997-2011 showed that approximately 50% of the 70 Western North Pacific TCs possessing double eyewalls went through eyewall replacement cycles (Yang et al. 2013). The eyewall replacement cycle begins when an outer wind maximum appears, which on average lasts ~36 hours according to previous airborne in situ wind measurements in the Atlantic Basin (Sitkowski et al. 2011). During the Rainband and Hurricane Intensity Experiment (RAINEX), airborne Doppler radars captured several snapshots of concentric eyewalls in Hurricane Rita (2005) with unprecedented ~500 m spatial resolution (Houze et al. 2007), where the three-dimensional structure of the double eyewalls was clearly illustrated (e.g. Bell et al. 2012; Didlake and Houze 2011). The double eyewall structure of Typhoon Saomai (2006) was sampled every six minutes over an eight-hour period by a coastal WSR-98D radar in China before landfall (Zhao et al. 2008). Zhao et al. first demonstrated the contraction of the outer eyewall and intensification of Saomai using the axisymmetric radar reflectivity, tangential winds, vertical vorticity, and pressure deficit derived from the ground-based velocity track display (GBVTD, Lee et al. 1999) technique. These studies suggested that concentric eyewalls are not necessarily two separate “closed” convective rings in the two-dimensional horizontal view and may be linked by “connecting bands” through a moat region while the rainbands spiral out and attach to the outer eyewall (e.g., Houze et al. 2007; Houze 2010). There are several recently proposed theories on secondary eyewall formation that include potential vorticity generation and accumulation at the rainband region (Judt and Chen 2010), vortex Rossby waves (Montgomery and Kallenbach 1997, Abarca and Corbosiero 2011; Menelaou et al. 2012), the formation of unbalanced supergradient wind (e.g., Huang et al. 2012, Abarca and Montgomery 2014), balance response and/or axisymmetrization of outer rainbands (e.g., Fang and Zhang 2012; Rozoff et al. 2012; Sun et al. 2013; Kepert 2013), and two-dimensional vortex interactions (Kuo et al. 2008).

Although double concentric eyewalls have been observed quite often in intense TCs, the presence of an incomplete tertiary eyewall has only been revealed by 85-GHz satellite radiance measurements from SSM/I and the in-situ wind measurements from the US Air Force C-130 Reconnaissance aircraft in Hurricane Juliette (2001) and Frances (2004) in the East Pacific basin (McNoldy 2004; Sitkowski et al. 2011). It is also possible that the tertiary eyewall occurs more often but is rarely sampled by either satellite or reconnaissance aircraft. The high temporal (every six minutes) and spatial (1 km) resolution Doppler radar data in Typhoon Usagi (2013) presented a unique opportunity to document the formation, evolution and three-dimensional structure of a triple eyewall during a 14-hour period before it made landfall in southeastern China. The radar loops is available online (see http://radar.nju.edu.cn/file/Usagi.mov).

Triple Eyewall Structure and Evolution in Usagi (2013)

Usagi possessed double eyewalls when it entered the Shantou WSR-98D radar (STRD) reflectivity range (~300 km) at 1900 UTC 21 September 2013 (Figure 1). A third maximum of radar reflectivity formed at ~100 km radius from the Usagi's center at ~2100 UTC 21 September 2013. The formation of a tertiary eyewall from 0200 to 0600 UTC is illustrated using 1.5° planposition-indicator (PPI) (Figure 2). Although the axisymmetric reflectivity in Figure 1 indicated that a tertiary eyewall signal formed about 5 hours earlier before 0200 UTC, the tertiary eyewall in Fig. 2a was originally composed of two cyclonically rotating, outward-propagating spiral rainbands connected to the secondary eyewall (e.g., 0200 UTC). These two rainbands formed a nearly closed eyewall at 0600 UTC. The two "moat" regions can be delineated and the eyewalls were connected by rainbands. The corresponding Doppler velocity (Figs, 2d, e, f) possessed three distinct velocity dipoles marked by dashed circles. All three eyewalls contracted with time (Fig. 1). From the reflectivity perspective, both the inner and secondary eyewalls did not dissipate after the formation of the tertiary eyewall, unlike a typical eyewall replacement cycle (ERC) event. As shown in Figure 1, the tertiary eyewall and the secondary eyewall first contacted the coastline at around 0600 and 0800 UTC, respectively; interaction with the land might have resulted in the interruption of the eyewall replacement cycles.

Shortly after 00 UTC 22 September, the Usagi's center entered the Doppler range (230 km) where the axisymmetric kinematic structure, vorticity, and pressure deficit can be deduced from the GBVTD methodology (Lee et al. 1999； 2000). The domain of the GBVTD analyses extends from the center of Usagi to 90 km radius and from 1 km to 12 km in the vertical with 1 km grid spacing in both the radial and vertical direction, consistent with the radar sampling resolution. The axisymmetric vertical structure of the triple eyewalls at 0600 UTC, derived from the GBVTD methodology, portrayed the secondary circulation of Usagi (Fig. 3). Each of the three eyewalls was accompanied by a clearly defined maximum of reflectivity, tangential wind, and updraft that was separated by a moat region (defined as a zone of weak precipitation or low reflectivity) in between. It is noted that the moats were primarily associated with weak downdraft and the air in the moat fed into eyewalls on both sides. Although having a weaker axisymmetric tangential wind than that associated with the secondary eyewall, the inner eyewall still possessed the strongest updraft. Both the secondary and tertiary eyewalls contracted with time, clearly illustrated in the time evolution of axisymmetric reflectivity and tangential winds, and vertical vorticity fields (Fig.1 and Fig. 4). The inner eyewall possessed a stable monopole vorticity pattern while the secondary and the tertiary eyewalls each possessed a barotropically unstable ring vorticity pattern. Shortly after the development of the tertiary eyewall (e.g., 00 UTC), the tangential winds of the inner and secondary eyewalls weakened between 00 and 02 UTC. The axisymmetric tangential wind of the inner eyewall remained steady after 02 UTC while the axisymmetric tangential winds within both the secondary and tertiary eyewalls increased as the eyewalls continued to contract with time (Fig. 4a). A corresponding sequence is also reflected in the pressure deficit (Fig. 4d) where the central pressure deficit first rose then dropped steadily, consistent with the evolution of the axisymmetric tangential wind field. Note that the increasing wind speed in the secondary eyewall may also be partially due to a better sampling of low-level structure as the Usagi moved closer toward the radar from 00 to 06 UTC. It is also interesting to note that in this event the inner eyewall did not dissipate as in a classical ERC but persisted even a few hours after the formation of the tertiary eyewall. The longevity of the inner eyewall will be the subject of a future study which might be related to the energy transported outward from Usagi's eye as illustrated by the low-level outflow from the eye (Fig. 3b). It is also possible that the closed secondary and tertiary eyewalls were broken after they reached the coastline.

Although, the inner eyewall remained quite steady during the analysis period, its peak axisymmetric tangential wind began to fade after 06 UTC (Fig. 4a) as the secondary eyewall continued to contract. The inner moat contracted consistently along with the secondary eyewall, began to be filled by precipitating clouds after 05 UTC, and lost its identity after 08 UTC when the inner moat reached the coastline (Fig. 1 and 4c), two hours behind the dissipation of the axisymmetric tangential wind maximum. The outer moat evolved in a similar manner. Each of the two moats was accompanied by weak downdraft sandwiched by two updrafts (Fig. 3b), consistent with previous aircraft in-situ and radar observations (e.g., Black et al. 1992 and Houze et al. 2007). Rozoff et al. (2006) argued that a rapid filamentation zone[3] was detrimental to convective development as a competing mechanism for moat formation. The radial minima of Usagi's filamentation time (Fig. 4e) were located radially outward from the axisymmetric tangential wind maxima where strain dominates vorticity. They were not collocated with the moats region (Fig. 4c and Fig. 4e). Therefore, the filamentation mechanism may not be the primary reason for the moat formation (e.g., Wang 2008), which may be related to the ERC as the rapid filamentation zone was located near the inner part of the moat and thus might suppress the convective activity there. It is also noted that the outer moat region might also be influenced by the land after 0600 UTC, which can affect the filamentaion process. Some recent idealized studies have shown that filamentation's potential detrimental impact on convection would be conditional on other factors, such as the amount of mid-level moisture, vertical wind shear impacts, and the presence or non-presence of other convective forcing mechanisms (e.g., Kilroy and Smith 2013, Kilroy et al. 2014). This topic is also worth of studying in the future.

Concluding Remarks

This study presents the first ever Doppler radar observations of a triple-eyewall typhoon, the formation of a tertiary eyewall, and the subsequent ERC in Usagi. The tertiary eyewall began

[3] The filamentation time is estimated based on the Okubo–Weiss eigenvalues describing the evolution of tracer gradient. A rapid filamentation zone is a region of strain-dominated flow where the filamentation time is smaller than the 30-min moist convective overturning time. Rozoff et al. (2006) argued that a rapid filamentation zone was detrimental to convective development as a competing mechanism for moat formation.

with two rainbands spiraling out from the secondary eyewall and then evolved into a nearly closed radar reflectivity ring. We highlight the axisymmetric structure and evolution of the primary and secondary circulations associated with each eyewall and moat. The inner eyewall began to dissipate after the formation of the tertiary eyewall and the rapid filamentation zone located outside of the eyewall axisymmetric tangential wind maximum might not be the primary mechanism for the moat formation. Several outstanding questions are: 1) what is the role of the tertiary eyewall, 2) why the inner eyewall did not dissipate after the formation of the secondary eyewall as reported in other ERC, 3) what is the relationship between the vorticity filamentation and the axisymmetrization process, and 4) how can the environmental factors and landfall process influence the filamention process? These detailed radar observations and the GBVTD-derived kinematic and dynamic properties are expected to provide a basis for future studies.

Acknowledgments. This work was primarily supported by the National Fundamental Research 973 Program of China (2013CB430101), the National Natural Science Foundation of China (grants 41322032, 41275031 and 41230421), and the Social Common Wealth Research Program (GYHY201006007).

For Further Readings

Abarca, S. F., and K. L. Corbosiero (2011): Secondary eyewall formation in WRF simulations of Hurricanes Rita and Katrina (2005): *Geophys. Res. Lett.*, 38, L07802, doi:10.1029/2011GL047015.

Abarca S. F. and M. T. Montgomery, 2014: Departures from Axisymmetric Balance Dynamics during Secondary Eyewall Formation. *J. Atmos. Sci.*, 71, 3723-3738.

Bell, M. M., M. T. Montgomery, and W.-C. Lee, 2012: An axisymmetric view of concentric eyewall evolution in Hurricane Rita (2005). *J. Atmos. Sci.*, 69, 2414–2432.

Black, M. L., and H. E. Willoughby, 1992: The concentric eyewall cycle of Hurricane Gilbert. *Mon. Wea. Rev.*, **120,** 947-957.

Didlake, A. C., Jr., and R. A. Houze, 2011: Kinematics of the secondary eyewall observed in Hurricane Rita (2005). *J. Atmos. Sci.*, **68,** 1620-1636.

Fang, J., and F. Zhang, 2012: Effect of beta shear on simulated tropical cyclones. *Mon. Wea. Rev.*, 140, 3327–3346.

Hawkins, J. D., M. Helveston, T. F. Lee, F. J. Turk, K. Richardson, C. Sampson, J. Kent, and R. Wade, 2006: Tropical cyclone multiple eyewall configurations. Preprints, 27th Conf. on Hurricanes and Tropical Meteorology.

Houze, R. A., Jr., 2010: Clouds in tropical cyclones. *Mon. Wea. Rev.*, **138,** 293-344.

Houze, R. A., Jr., S. S. Chen, B. F. Smull, W.-C. Lee, M. M. Bell, 2007: Hurricane intensity change and eyewall replacement. *Science*. **315,** 1235-1239.

Huang, Y.-H., M. T. Montgomery, and C.-C. Wu, 2012: Concentric eyewall formation in typhoon Sinlaku (2008). Part II: Axisymmetric dynamical processes. *J. Atmos. Sci.*, 69, 662–674, doi:10.1175/JAS-D-11-0114.1.

Judt, F., and S. S. Chen, 2010: Convectively generated potential vorticity in rainbands and formation of the secondary eyewall in Hurricane Rita of 2005. *J. Atmos. Sci.,* 67, 3581–3599.

Kepert, J. D., 2013: How does the boundary layer contribute to eyewall replacement cycles in axisymmetric tropical cyclones? *J. Atmos. Sci.,* 70, 2808–2830, doi:10.1175/JAS-D-13-046.1.

Kuo, H.-C., W. H. Schubert, C.-L. Tsai, and Y.-F. Kuo, 2008: Vortex interactions and barotropic aspects of concentric eyewall formation. *Mon. Wea. Rev.*, 136, 5183–5198.

Kuo, H. C., C. P. Chang, Y. T. Yang, and H. J. Jiang, 2009: Western North Pacific Typhoons with Concentric Eyewalls. *Mon. Wea. Rev.*, 137, 3758–3770.

Lee, W.-C., J.-D. Jou, P.-L. Chang, and S.-M. Deng, 1999: Tropical cyclone kinematic structure retrieved from single Doppler radar observations. Part I: Interpretation of Doppler velocity patterns and the GBVTD technique. *Mon. Wea. Rev*., **127,** 2419-2439.

Lee, W.-C., J.-D. Jou, P.-L. Chang and F. D. Marks, 2000: Tropical cyclone kinematic structure retrieved from single-Doppler radar observations. Part III: Evolution and structure of Typhoon Alex (1987). *Mon. Wea. Rev.*, **128,** 3892-4001.

McNoldy, B. D., (2004): Triple Eyewall in Hurricane Juliette. *Bull. Amer. Meteoro. Soc.,* 1663-1666.

Menelaou, K., M. K. Yau, and Y. Martinez (2012): On the dynamics of the secondary eyewall genesis in Hurricane Wilma (2005), *Geophys. Res. Lett.*, 39, L04801, doi:10.1029/2011GL050699.

Montgomery, M. T. and R. J. Kallenbach, 1997: A theory for vortex Rossby-waves and its application to spiral bands and intensity changes in hurricanes. *Q. J. R. Meteorol. Soc.*, 123, 435-465.

Rozoff, C. M., W. H. Schubert, B. D. McNoldy, and J. P. Kossin, 2006: Rapid filamentation zones in intense tropical cyclones. *J. Atmos. Sci.*, 63,325–340.

Rozoff, C. M., D. S. Nolan, J. P. Kossin, F. Zhang, and J. Fang, 2012: The roles of an expanding wind field and inertial stability in tropical cyclone secondary eyewall formation. *J. Atmos. Sci.*, 69, 2621–2643.

Sitkowski, M., J. Kossin, and C. M. Rozoff, 2011: Intensity and structure changes during hurricane eyewall replacement cycles. *Mon. Wea. Rev.*, 139, 3829-3847. doi: http://dx.doi.org/10.1175/MWR-D-11-00034.1

Sun, Y. Q., Y. Jiang, B. Tan, and F. Zhang, 2013: The governing dynamics of the secondary eyewall formation of Typhoon Sinlaku (2008). *J. Atmos. Sci.*, 70, 3818–3837, doi:10.1175/JAS-D-13-044.1.

Willoughby, H. E., J. Clos, and M. Shoribah, 1982: Concentric eyewalls, secondary wind maxima, and the evolution of the hurricane vortex. *J. Atmos. Sci.*, **39,** 395-411.

Wang, Y., 2008: Rapid filamentation zone in a numerically simulated tropical cyclone. *J. Atmos. Sci.*, 65, 1158–1181.

Yang, Y.-T., H.-C. Kuo, E. A. Hendricks, and M. S. Peng, 2013: Structural and intensity changes of concentric eyewall typhoons in the western North Pacific basin. *Mon. Wea. Rev.*, 141, 2632–2648, doi:10.1175/MWR-D-12-00251.1.

Zhao, K., W.-C. Lee, and B. J.-D. Jou (2008), Single Doppler radar observation of the concentric eyewall in Typhoon Saomai, 2006, near landfall, *Geophys. Res. Lett.*, 35, L07807, doi:10.1029/2007GL032773.

Figure Captions

Figure 1. The axisymmetric reflectivity of typhoon Usagi from 1800 UTC 21 September to 1800 UTC 22 September 2013. The inset indicates the best track of Usagi (solid line with typhoon symbols). Range rings indicate maximum Doppler coverage (230 km) for ShanTou (STRD) CINRAD WSR-98D radar.

Figure 2. Radar reflectivity (a-c) and radial velocity (d-f) at 1.5º elevation from three analysis times (0200, 0400, and 0600UTC) observed by STRD. The dashed circles indicate the eyewall positions. The arrows represent the direction toward the STRD. The black solid lines indicate the coastal line.

Figure 3. Radius-height cross-section of the azimuthal mean structure at 0600 UTC. Color represents reflectivity in dBZ; contours in (a) are mean tangential wind (m s^{-1}), Vectors in (b) indicate mean secondary circulation. The black triangle represents the position of the nearest coastline.

Figure 4. Radial profiles at 2km height for five analysis times (0000, 0200, 0400, 0600 and 0800UTC). Different line colors represent analysis times; (a) mean tangential wind (ms^{-1}), (b) mean vertical vorticity ($10^{-3}s^{-1}$), (c) mean reflectivity (dBZ),(d) perturbation pressure deficit (hPa) assuming zero at 90 km radius and (e) filamentation time (min). Analysis domain extends to 90 km radius.

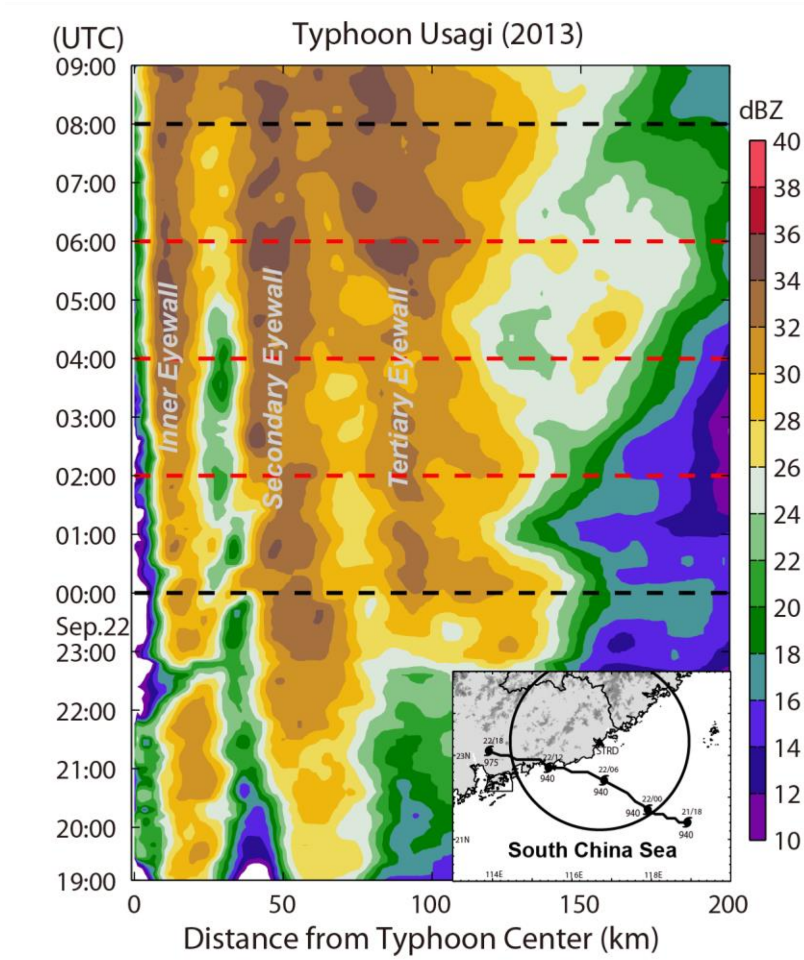

Figure 1. The axisymmetric reflectivity of typhoon Usagi from 1800 UTC 21 September to 1800 UTC 22 September 2013. The inset indicates the best track of Usagi (solid line with typhoon symbols). Range rings indicate maximum Doppler coverage (230 km) for ShanTou (STRD) CINRAD WSR-98D radar.

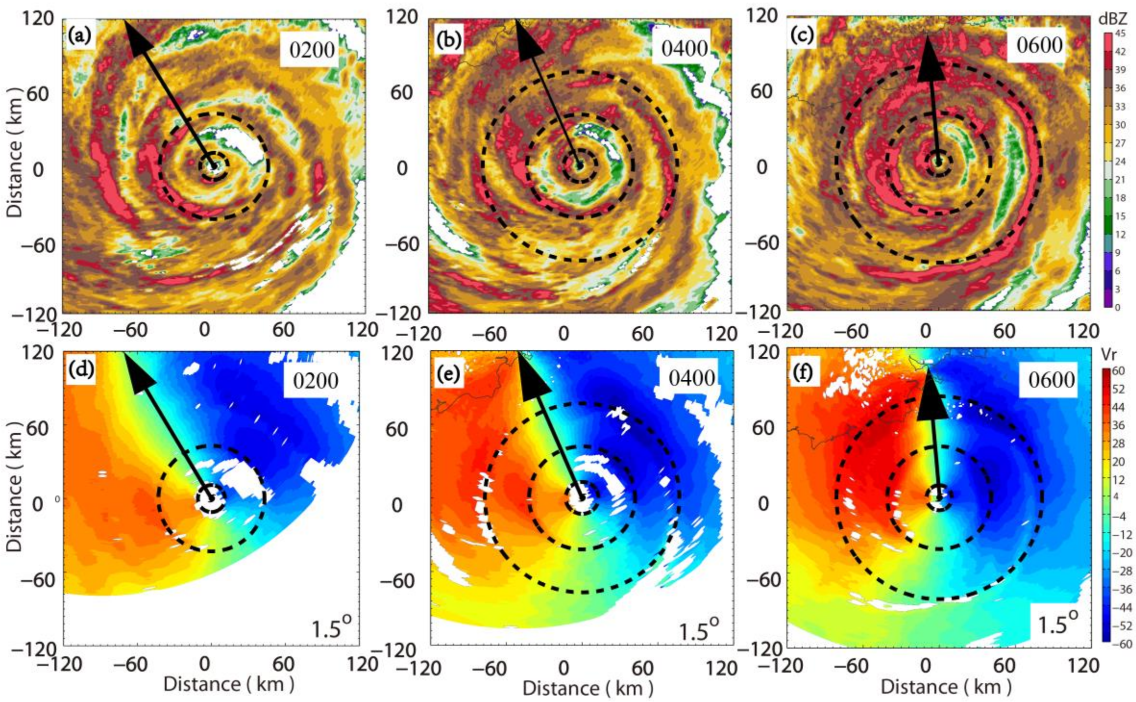

Figure 2. Radar reflectivity (a-c) and radial velocity (d-f) at 1.5° elevation from three analysis times (0200, 0400, and 0600UTC) observed by STRD. The dashed circles indicate the eyewall positions. The arrows represent the direction toward the STRD. The black solid lines indicate the coastal line.

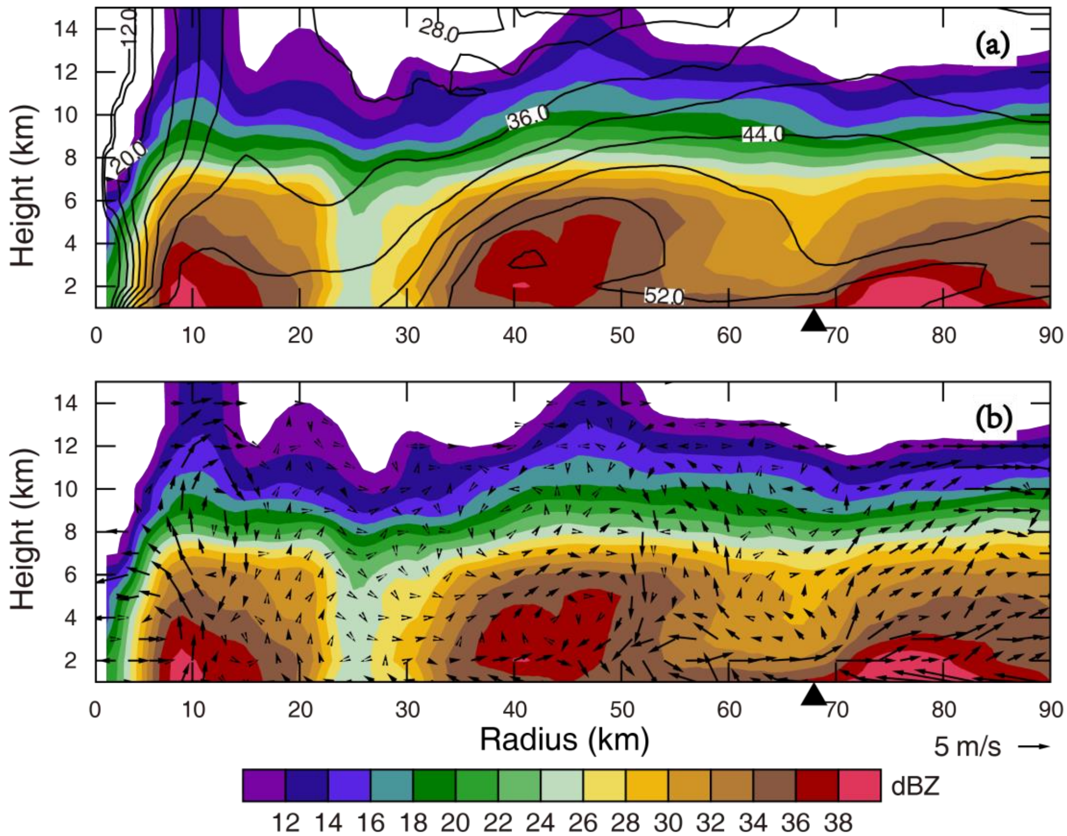

Figure 3. Radius-height cross-section of the azimuthal mean structure at 0600 UTC. Color represents reflectivity in dBZ; contours in (a) are mean tangential wind (m s^{-1}), Vectors in (b) indicate mean secondary circulation. The black triangle represents the position of the nearest coastline.

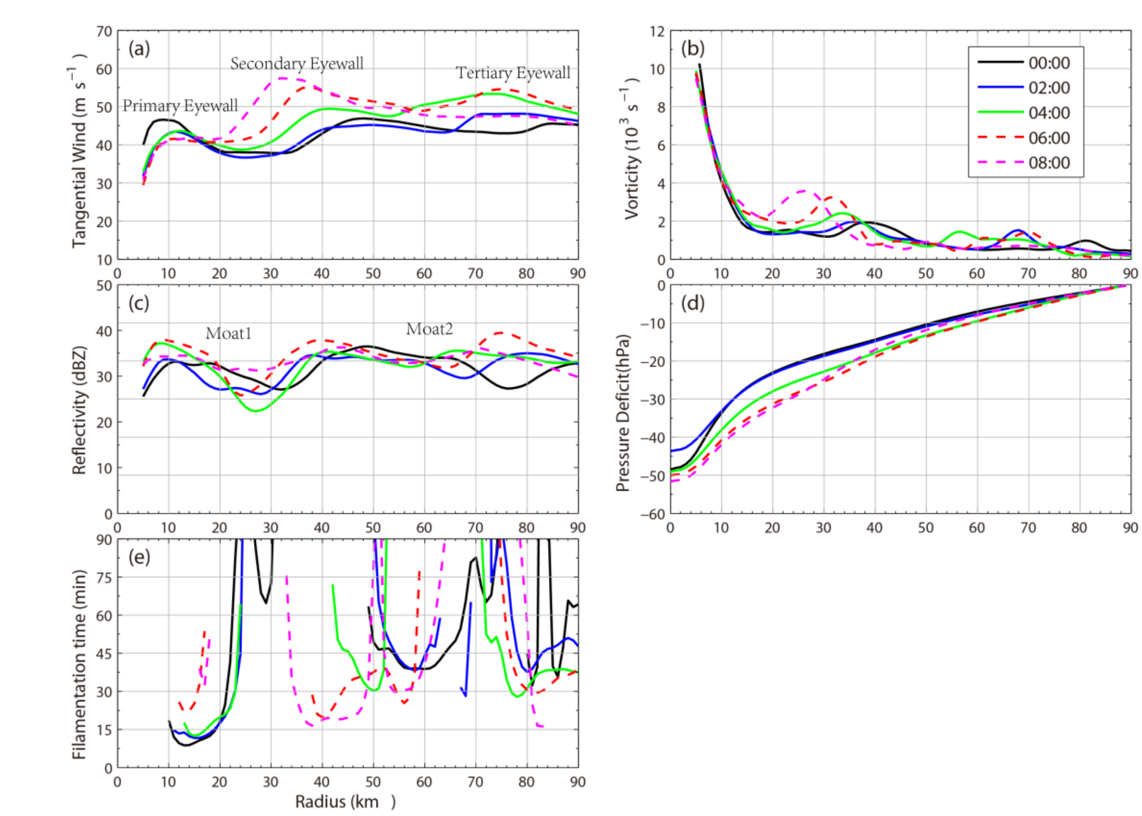

Figure 4. Radial profiles at 2 km height for five analysis times (0000, 0200, 0400, 0600 and 0800 UTC). Different line colors represent analysis times; (a) mean tangential wind (m s^{-1}), (b) mean vertical vorticity (10^{-3} s^{-1}), (c) mean reflectivity (dBZ), (d) perturbation pressure deficit (hPa) assuming zero at 90 km radius and (e) filamentation time (min). Analysis domain extends to 90 km radius.